PHYSICAL REVIEW C VOLUME 47, NUMBER 5 MAY 1993

Thermal characteristics of composite systems formed in fusion of ^{28}Si with ^{118}Sn and ^{124}Sn nuclei

J. L. Wile,* S. S. Datta,† W. U. Schröder, J. Tõke, D. Pade,‡ S. P. Baldwin,
J. R. Huizenga, B. M. Quednau, R. T. deSouza,§ and B. M. Szabo
Department of Chemistry and Nuclear Structure Research Laboratory, University of Rochester,
Rochester, New York 14627

(Received 30 June 1992)

Neutrons from the fusion reactions of 120–150 MeV ^{28}Si with ^{118}Sn and ^{124}Sn target nuclei have been measured in coincidence with evaporation residues, in two series of complementary experiments using either a 4π neutron multiplicity meter or a neutron time-of-flight spectrometer. Both the energy spectra and multiplicity distributions reveal significant quantitative differences in the decay patterns of the compound nuclei ^{146}Gd and ^{152}Gd formed in the two reactions studied. It is shown that these differences cannot be understood in terms of decay cascades proceeding through states of enhanced collective energy, such as the superdeformed states, suggested in earlier studies. Instead, they can be explained consistently within the framework of a statistical decay model, if different effective level density parameters are allowed for the evaporation chains of the two composite systems.

PACS number(s): 25.70.Jj, 25.70.Gh

I. INTRODUCTION

Heavy-ion induced fusion or fusionlike reactions have proven to be powerful tools for the population of nuclear states in a wide range of excitation energies and spins [1–4]. Studies of the properties of such states have contributed significantly to an understanding of the interplay between nuclear structure and dynamics. In such investigations, the statistical model plays a key role, providing a link between the properties of nuclear matter, on the one hand, and experimental observables such as, e.g., the multiplicity and energy distributions of emitted particles or γ rays, on the other hand.

In a number of experiments, considerable effort has been devoted [5–14] to the exploration of particle and γ-ray multiplicities associated with evaporation residues in the lanthanide region, just above the $N = 82$ closed shell. Various observations have been made [6–13] of abnormal developments with excitation energy and entrance-channel spin of particle multiplicities associated with the production of Er and Gd isotopes in (^{28}Si,$xnyp$) and (^{64}Ni,$xnyp$) reactions. For example, the experimental particle multiplicities for the reaction ^{124}Sn+^{28}Si at various bombarding energies were found by Stwertka *et al.* [7,8] to be systematically lower than predicted by statistical evaporation codes, employing sets of input parameters established in earlier studies covering a wide range of nuclear systems. In related work, Janssens *et al.* [11] have studied the two systems ^{92}Zr+^{64}Ni and ^{144}Sm+^{12}C leading to the same ^{156}Er compound nucleus with excitation energies ranging from 30 to 70 MeV. It was noted in their study that, while the statistical model describes quite accurately the average multiplicities of neutrons from the asymmetric, ^{12}C-induced reaction, it systematically underpredicts the emission of neutrons from the more symmetric, ^{64}Ni-induced reaction. In order to explain such differences between the decay patterns of the same system formed in two different ways, the possible role of superdeformed bands embedded in the continuum above the yrast line [6–14] and of preequilibrium particle emission in limiting the excitation energy available for particle evaporation have been considered. While the latter process was shown to be insignificant at the bombarding energies of interest here [2], the presence of superdeformed (SD) bands has been confirmed experimentally for the lanthanide [15,16] and mercury [17] regions. Some nuclides have been observed to possess up to six different SD bands. The relative populations of individual bands have been found typically of the order of only 0.01, i.e., by far too small to explain the above differences in the particle evaporation patterns. Although entrance channel effects have been observed [18,19] for the population of SD bands, measurements [20,21] of charged-particle energy spectra associated with different bands of excited states have, thus far, not provided consistent evidence for the influence of nuclear structure on the decay of compound nuclei in the mass regions $A = 80$–90 and $A = 130$–150. In any case, a population of SD bands or an excitation of other “slow” collective degrees of freedom with a combined probability of at least 0.1 would be required to enable this process to influence the particle decay patterns noticeably. Such higher probabilities exceeding equilibrium-statistical predictions would imply quite a strong memory of the entrance channel and, hence, contradict the notion of a “normal” equilibrated compound system.

The present work, which is a part of a systematic study

---

*Present address: Ball State University, Muncie, IN 47306.

†Deceased.

‡Present address: Dornier GmbH, Friedrichshafen, Germany.

§Present address: Indiana University Cyclotron Facility, Bloomington, IN 47408.

of compound-nucleus formation and decay phenomena, attempts to shed light on the apparently puzzling inconsistencies with statistical-model calculations reported [5–9,12,13] for neutron emission in the fusion reactions of ^{28}Si with ^{118}Sn and ^{124}Sn nuclei. Two series of complementary experiments are reported, in which neutron energy spectra and multiplicity distributions were measured in coincidence with evaporation residues (ER) at various bombarding energies, in order to provide a stringent test of the validity of a statistical-model description for the decay of the composite systems formed in these two reactions. Experimental techniques employed in the two series of experiments are described in Sec. II, while results are discussed in Sec. III. Summary and conclusions are presented in Sec. IV.

II. EXPERIMENTAL TECHNIQUES

The experiments were performed at the Emperor tandem Van de Graaff accelerator of the University of Rochester Nuclear Structure Research Laboratory, using two different experimental setups. As described in Sec. II A, in the first type of experiment a high-efficiency neutron multiplicity meter was used to count neutrons, while evaporation residues were measured using silicon detectors. The second setup, described in Sec. II B, utilized a neutron time-of-flight (TOF) spectrometer in conjunction with the Rochester recoil mass spectrometer (RMS). Bombarding energies ranged from $E_{\mathrm{lab}}=120$ MeV to 150 MeV. Targets were isotopically enriched, 100–200 μg/cm^2 thick, either self-supporting or evaporated onto thin (10–15 μg/cm^2) carbon backings.

A. Measurements of exclusive neutron multiplicity distributions

The experimental setup for measuring event by event the multiplicity of neutrons coincident with evaporation residues is shown schematically in Fig. 1. The experimental procedure [22–26], novel to heavy-ion induced fusion reaction studies, utilizes a high-efficiency neutron multiplicity meter (NMM) in conjunction with two silicon heavy-ion (evaporation residue) detectors (SSD) placed at forward angles. As the target is located in the center of the NMM, the latter subtends a solid angle of virtually a 4π for reaction neutrons.

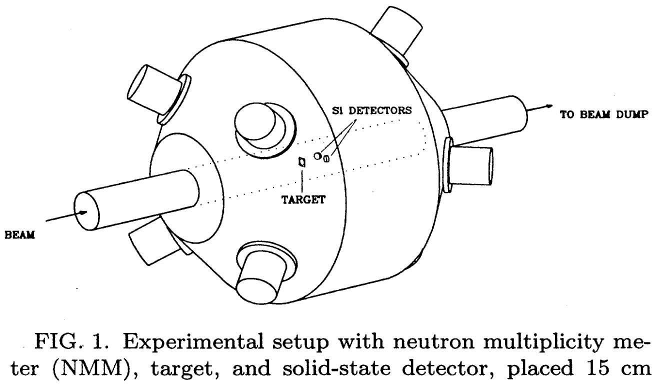

FIG. 1. Experimental setup with neutron multiplicity meter (NMM), target, and solid-state detector, placed 15 cm downstream of the target.

The NMM is a 900 l tank of approximately spherical shape, filled with gadolinium-loaded (0.2% by weight) organic scintillator NE224 viewed by eight RCA-4522 photomultipliers. The principle of operation of such a detector hinges on a statistically delayed response of the scintillator to individual neutrons, so as to allow one to count electronically one by one, each of the reaction neutrons injected simultaneously into the detector volume. This principle is discussed in more detail elsewhere [22–26]. The characteristic parameter of the NMM most crucial for data reduction is the neutron detection probability. This probability depends not only on the geometry of the device, position of the target, and electronic thresholds, but also on the velocity vector of each neutron, and hence depends on the reaction studied. Additionally, due to the high counting efficiency of the device, there are background counts present that have to be accounted for. Therefore, the soundest approach in interpreting the "raw" NMM data appears to consist in their comparison with theoretical model predictions folded with both the detector response and the empirical background multiplicity distribution. However, in the case of a simple reaction mode and a high-efficiency device, such as in the present experiment, alternative methods, in which the measured multiplicities are first corrected for background and then for the calculated efficiencies, prove accurate in Monte Carlo simulation calculations. Such an approach, pursued in the present study, offers the advantage of providing event-by-event (approximate) values of the experimental true multiplicities.

The NMM response to neutrons from fusion reactions was calculated with a modified version of the Monte Carlo code DENISW [27]. This type of calculation was calibrated earlier by using measured neutron multiplicities for a ^{252}Cf fission source placed at various positions along the NMM axis and comparing them with the known neutron multiplicity distribution for this source. In the present experiment, the NMM had an efficiency of 78% for ^{252}Cf fission neutrons, to a large extent determined by the electronic threshold set to achieve a compromise between efficiency and background counting rate. The efficiency calculations using the code DENISW proved accurate also in tests of the NMM using ^{16}O-induced fusion reactions on tin targets, and the fusion reaction ^{12}C+^{28}Si. These calculations were also tested for a more complex setup used in a study of the damped reaction ^{165}Ho+^{56}Fe [26].

The multiplicity of background counts in the NMM was measured event by event, in order to account for the possibly large fluctuations due mostly to the instabilities of intensity and spot position of the beam on the target. For this purpose, for each event, NMM signals were processed in two counting intervals of 128 μs length each, separated by 472 μs. The first counting interval was started 100 ns after detection of the reaction event, in order to avoid counting prompt signals from the NMM associated with reaction γ rays and recoil protons from the fast neutron moderation processes. During this interval, detected signals were due mostly to the reaction neutrons, with a small contamination with background sources. During the second counting interval, started 600 μs after the detection of the reaction event, no neutrons from that event were present any more, and all signals were attributable to the background sources. The main source of NMM background signals were γ rays and neutrons from additional reactions induced by the beam in the target, for which the associated charged products remained undetected. In the experiment, beam intensities were limited so as to keep the background counting rate as low as 0.2–0.5 per counting interval. Additionally, detection times of all NMM signals were recorded individually, employing unique multistop TDC modules [28], which allowed one to optimize the effective width of the counting interval in an off-line analysis.

In order to distinguish evaporation residues (ER) from other charged reaction products, a time-of-flight (TOF) method was employed. The start signal for the TOF measurement was derived from the prompt NMM signal associated with an event detected in one of the two silicon detectors. The stop signals for the TOF measurement, as well as the charged-product energy signals, were provided by the latter silicon detectors. The resolution of this energy-TOF measurement was sufficient to distinguish evaporation residues from the reactions of interest from charged products of a different origin. Most notably, the effective NMM-silicon detector coincidence requirement imposed by the TOF measurement allowed one to reject elastic-scattering events that would otherwise have flooded the acquisition system, which was operated with a large busy time required by the gadolinium-loaded scintillator NMM. It is important to note that the efficiency of the NMM for detecting at least one of the 10–30 low-energy prompt γ rays [8], emitted typically in a fusion-evaporation reaction, is essentially unity for all significant γ multiplicities. This method of event triggering, hence, does not lead to any noticeable biasing of the acquired events.

As an example of data acquired with the NMM setup, two-dimensional scatter plots of TOF vs energy are shown in Fig. 2, for events from the reactions of 160-MeV ^{28}Si projectiles with a ^{12}C target (left), and with a ^{124}Sn target and its ^{12}C backing (center). There are clearly two groups of events distinguishable in the center plot, associated with the ^{124}Sn + ^{28}Si and ^{12}C + ^{28}Si reactions, respectively. This figure demonstrates that events related to fusion reactions of Si with Sn or C, as well as other backgrounds, are easily identified in the present experiment. On the right-hand panel of Fig. 2, a two-dimensional contour diagram of TOF vs neutron multiplicity is shown. The contributions due to the ^{124}Sn and the ^{12}C backing are clearly distinguished also in this representation of data. As expected, the Sn+Si fusion reaction, leading to a more neutron-rich and highly excited Gd, results in higher neutron multiplicities than the fusion of ^{12}C with ^{28}Si.

The ER detectors were located at $\theta=\pm6°$. With an angular acceptance of $\Delta\theta=5°$, these detectors presented an effective solid angle of approximately 12% of 4π for the (kinematically focused) ER's of interest. As illustrated in Fig. 3, this geometrical efficiency depends on the evaporation channel and, hence, has to be accounted for in a detailed data analysis. In this figure, theoretical ER angular distributions calculated with the code PACE [29] are shown for the 0n, 1n, 2n, 3n, and 4n decay channels of the composite system formed in the ^{118}Sn + ^{28}Si reaction at $E_{\rm lab}$=120 MeV. The limited angular range of ER detection, indicated by vertical arrows in this figure, leads to a higher rejection or miss rate for events with low neutron multiplicities, as compared with events of higher neutron multiplicity. This effect results typically in an approximately 5% increase in observed average neutron multiplicity, a bias which has been taken into account in the analysis and interpretation of data.

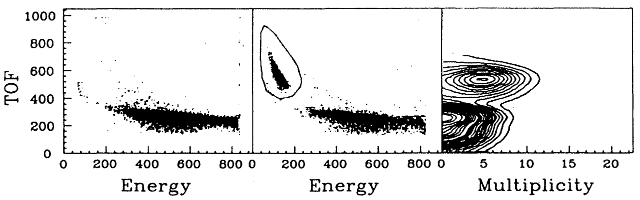

FIG. 2. Distributions of time of flight (TOF) vs energy of evaporation residues (left-most and center scatter plots), and of TOF vs multiplicity of the coincident neutrons (right-most contour diagram), for the reactions of 120-MeV ^{28}Si with ^{12}C (left panel) and carbon-backed ^{124}Sn targets (center and right panels).

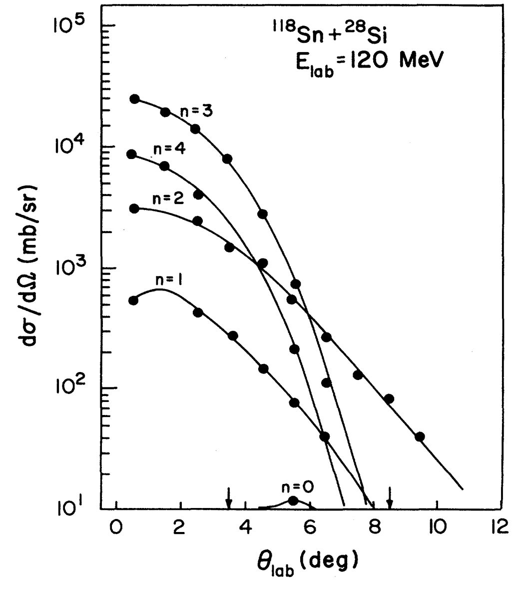

FIG. 3. Differential cross section $d\sigma/d\Omega$ vs angle $\theta_{\rm lab}$ for ER's from the ^{118}Sn+^{28}Si reaction at $E_{\rm lab}$=120 MeV, associated with evaporation of $n \leq 4$ neutrons. The vertical arrows indicate the limits of angular acceptance of the ER detectors.

B. Inclusive and exclusive neutron energy spectra

In the second series of experiments reported in the present work, energy spectra and angular distributions of neutrons from the fusion reactions of interest were measured both in a singles mode and in coincidence with evaporation residues, using a TOF method.

The setup used in this type of experiment is schematically illustrated in Fig. 4. The neutron TOF spectrometer consisted of 10 or 11 fast NE213 liquid-scintillator detectors, incorporating Amperex XP2041 photomultipliers and operated in conjunction with pulse-shape discriminator modules. The latter modules, developed by HMI-Elektronik, allowed one to distinguish very efficiently between detector signals due to neutrons and γ rays. Two of the detectors, placed in close vicinity of the target, were set up to provide the start signals for the TOF measurement by detecting prompt reaction γ rays. The remaining NE213 detectors were placed at distances of about 1 m from the target and at angles between 31.5° and 90°, in the case of the ^{124}Sn target, and between 40° and 130°, in the case of the ^{118}Sn target. These detectors were set up to detect neutrons and, therefore, to provide stop signals for the TOF measurement.

The TOF measurement, hence, required a γ-neutron coincidence, a necessity in cases of a structureless (DC) beams like the one from the Rochester tandem accelerator. Such a coincidence requirement not only affects adversely the useful count rate but has the potential of biasing the acquired events. Due to the fact that the start signals for the TOF measurement and, hence, the event acquisition triggers were generated by prompt γ rays measured with low-efficiency γ detectors, the acquired data are weighted approximately linearly with the multiplicity of low-energy γ rays, emitted from the evaporation residues at the end of their decay cascades. Fortunately, the γ multiplicities and energies are known [8] for some of the individual Gd ER's of interest here, produced in ^{28}Si-induced reactions under very similar conditions. From a consistently rather weak dependence of the γ multiplicity on the energy of a detected γ ray and a concentration of the spectra at low γ energies, where the γ detectors have their maximum efficiency, one expects the above γ-n coincidence requirement not to lead to any noticeable bias in the data of the type presented here.

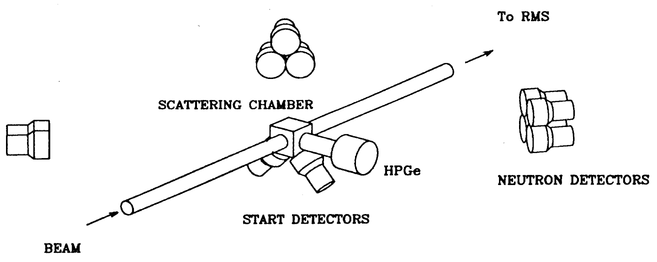

FIG. 4. Schematic diagram of the neutron TOF setup with two start (γ) detectors and nine stop (neutron) detectors. An additional HPGe detector was used to identify ER's by their characteristic γ rays. ER's are identified in mass by a recoil mass spectrometer (RMS).

A superposition of γ and neutron TOF spectra is shown in Fig. 5, as measured with one neutron detector and both start γ detectors. The two narrow peaks below channel number 200 are due to prompt γ rays detected in the stop detector and in either of two start detectors. The time resolution inferred from these narrow γ-γ coincidence peaks is approximately 0.7 ns. As seen from this figure, the random background in the TOF spectrum was negligibly low. Additional test measurements, in which 10-cm-diam and 33-cm-long steel "shadow bars" were placed in front of two of the neutron detectors, showed that contamination of the TOF spectra by scattered neutrons was of no significance in the experiment. In principle, distortions of the TOF spectra could be induced by delayed γ rays from the decay of isomeric states, starting the neutron TOF measurement. However, in the present experiment, effects of this kind were found to be unimportant, as illustrated by the rather symmetric shape of the γ-γ coincidence line in the ^{118}Sn+^{28}Si TOF spectrum shown in Fig. 5. Delayed γ rays starting the TOF measurement with significant probability would have produced tail on the left-hand side of the γ-γ coincidence peak. In the experimental TOF spectra for either system, no indication is found of such a tail exceeding 1% in intensity relative to the γ-γ peak.

The time-of-flight (TOF) data were used to calculate the neutron kinetic energies. The obtained "raw" laboratory energy spectra were then corrected for the neutron detection efficiency [30], which depends on neutron energy, scintillator geometry, and electronic signal threshold. The latter threshold corresponded to approximately 0.5 MeV of recoil-proton energy. Finally, the corrected laboratory spectra were transformed into the c.m. frame of reference. The above procedure, which involves calculation of detection efficiencies and several data conversions, was tested using the experimental data from an experiment with the same TOF setup, however, with the target replaced by a 1 μCi ^{252}Cf fission/neutron source.

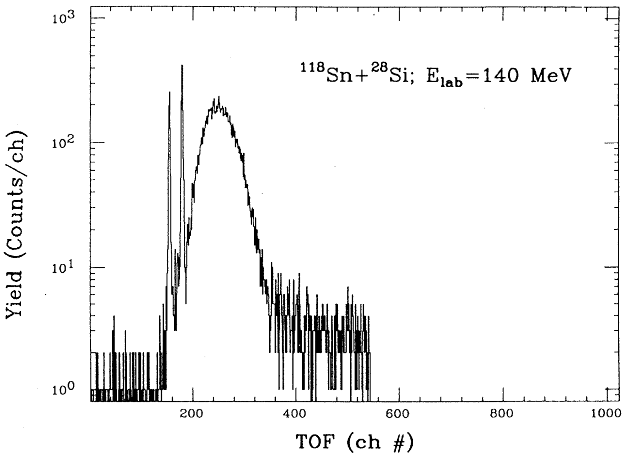

FIG. 5. Typical TOF spectrum from the 140-MeV ^{118}Sn+^{28}Si reaction. The two narrow peaks on the left are due to γ rays detected in both start and stop detectors, while the broad distribution at higher TOF's is due to neutrons.

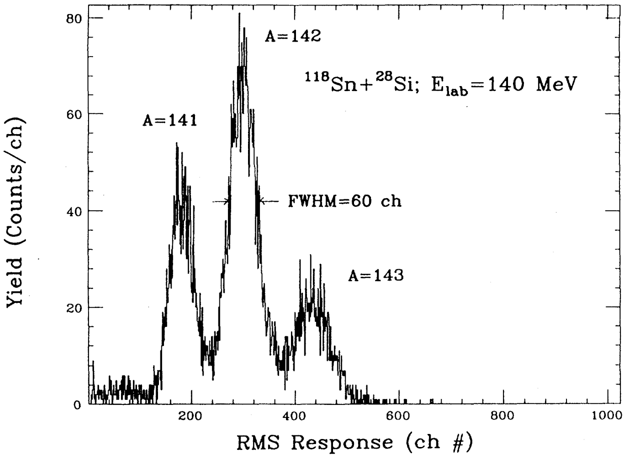

FIG. 6. Mass spectrum of ER's from the reaction ^{118}Sn+^{28}Si at $E_{\rm lab}$=140 MeV.

In this test experiment, energy spectra and multiplicities of neutrons coincident with the spontaneous fission fragments were determined and found in excellent agreement with published data for the ^{252}Cf nuclide [31].

In this second series of experiments, exclusive neutron data were collected in coincidence with evaporation residues detected and identified in the Rochester Recoil Mass Spectrometer (RMS) [32]. Such an exclusive measurement of neutron spectra required a triple coincidence between signals from start (γ) and stop (neutron) detectors, and from the RMS focal-plane detector and, hence, could be carried out only with a very low count rate. Because of this low count rate, such exclusive measurements were performed only at $E_{\rm lab}$=140 MeV for the ^{118}Sn target and at $E_{\rm lab}$=120 and 140 MeV in the case of the ^{124}Sn+^{28}Si reaction.

A typical mass spectrum of evaporation residues from the ^{118}Sn+(140 MeV)^{28}Si reaction, detected in the position-sensitive silicon focal-plane detector of the RMS, is shown in Fig. 6. Here, three groups of ER with mass numbers of A = 141–143 are clearly distinguished, with a resolution characteristic of the RMS, as set up for the present experiment. An even better mass separation than that seen in Fig. 6 can be achieved by using a two-dimensional representation of energy vs position of the data from the RMS focal-plane detector. In order to ascertain the validity of the RMS calibration and, hence, of the mass number assignment of the peaks in the ER energy spectra, characteristic γ rays of the ER's were detected using a high-purity germanium (HPGe) detector placed near the target.

III. RESULTS AND DISCUSSION

In the following, experimental results for the multiplicity distributions and energy spectra of neutrons emitted in the ^{118}Sn + ^{28}Si and ^{124}Sn + ^{28}Si fusion reactions are presented and discussed in terms of a statistical evaporation model. As the decay of the composite system formed in the reaction ^{118}Sn + ^{28}Si was found in earlier studies [7] to follow the general systematics of fusion-evaporation reactions in the energy domain of interest here, the study of this system served to a certain extent as a means of calibration or verification of the experimental and analysis method used in the present study. Such a "calibration" of the rather complex experimental method adds credibility to the conclusions reached in the exploration of the anomalies reported earlier [6,7,11] for the ^{124}Sn + ^{28}Si reaction.

A. The ^{118}Sn + ^{28}Si reaction

Experimental results obtained in the two series of experiments on the ^{118}Sn +^{28}Si reaction, as well as results of respective theoretical calculations, are shown in Figs. 7–10. In Fig. 7, multiplicity distributions $P(n)$ of neutrons from this reaction are shown, as measured with the NMM in coincidence with ER's. The solid histograms in this figure represent experimental results obtained at $E_{\rm lab}$=130, 140, and 150 MeV and correspond to excitation energies between E^*=60 and 90 MeV. These multiplicities have only been corrected for background. Statistical uncertainties of the experimental results, indicated by error bars, are small compared to systematical errors associated with calculations of detection probabilities. The dashed curves represent the results of evaporation calculations, using the code PACE [29]. These calculations used values of the model parameters based on systematics of compound-nuclear decay widths established

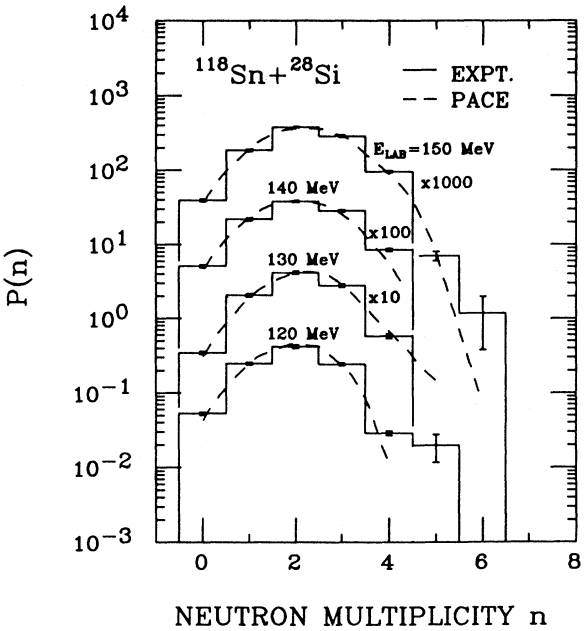

FIG. 7. Observed neutron multiplicity distributions $P(n)$, for the ^{118}Sn+^{28}Si reaction at $E_{\rm lab}$=120–150 MeV (histograms) and results of theoretical calculations using the code PACE (dashed), folded with neutron detection probability and angular acceptance function of the silicon detector.

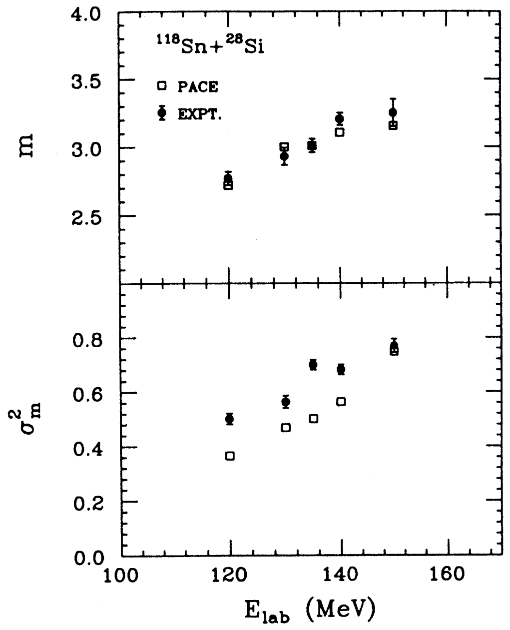

FIG. 8. Bombarding-energy dependence of the experimental (solid symbols with error bars) first and second moments of the neutron multiplicity distribution for the ^{118}Sn + ^{28}Si reaction extrapolated to 4π. The open symbols represent PACE calculations.

for the mass region of interest. In particular, the crucial nuclear level density parameter a has been assumed to scale with the mass number A according to $a = A/8$ MeV^{-1}. The theoretical distributions, corrected for neutron detection efficiency of the NMM and for the incomplete angular acceptance of the ER detectors, are seen to reproduce the data for the most probable deexcitation channels quite accurately. Only for the very highest multiplicities associated with rare decay channels, the simulation calculations fail to reproduce the experimental data quantitatively.

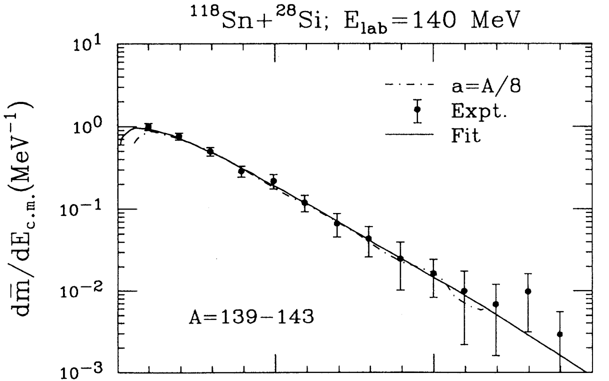

FIG. 9. Angle-integrated energy spectrum of neutrons (solid symbols) associated with ER's with A = 139–143, produced in the ^{118}Sn + ^{28}Si reaction at $E_{\rm lab}$=140 MeV. The solid curve is a fit with Eq. (1), the dash-dotted curve represents a PACE calculation with $a = A/8$ MeV^{-1}.

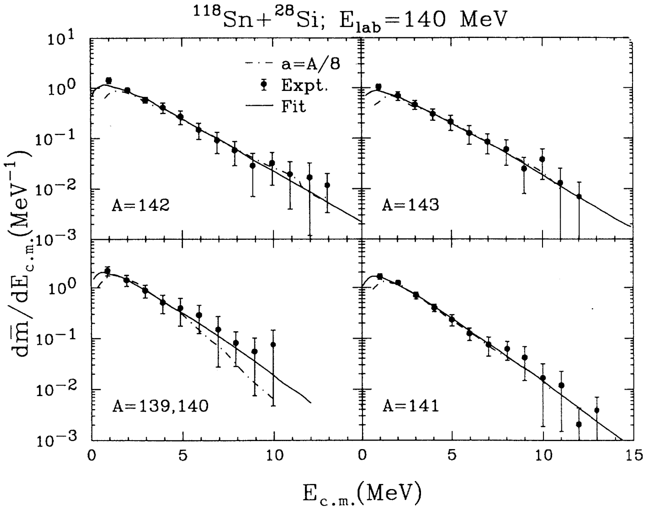

FIG. 10. Angle-integrated energy spectra of neutrons from individual ER's, identified by mass A in each panel, from the reaction ^{118}Sn + ^{28}Si at $E_{\rm lab}$=140 MeV. Symbols and curves have the same meaning as in Fig. 9.

A different quantitative comparison between experimental results, corrected for the detection efficiencies of both neutrons and evaporation residues, and the simulation calculations is shown in Fig. 8. In this figure, values of first two central moments, average values and variances, of the multiplicity distribution of neutrons in coincidence with ER's are displayed as functions of the bombarding energy. Here, the average experimental (solid dots) multiplicities are observed to be well explained by the statistical-decay calculations, over the whole bombarding-energy range explored. Theoretical model calculations are also seen to explain the trends in evolution of the second moment of the neutron multiplicity distribution with the bombarding energy, although the predicted values lie systematically somewhat below the measured ones. The origin of the small but systematic discrepancies is most likely to be found in numerous simplifying assumptions made in the computational implementation of the statistical model. Most notably, the theoretical calculations depend strongly on the assumed values of the effective level density parameter a, which may well show significant deviations from the simple "average" $a = A/8$ MeV^{-1} scaling. In particular, the underestimation of the experimental probabilities for high multiplicities points to a possible decrease in magnitude of a for the neutron-poor Gd isotopes.

It was one of the aims of the neutron TOF experiments to provide an independent and more sensitive measure of the crucial level density parameter. Results of these experiments for the ^{118}Sn+^{28}Si system are shown in Figs. 9 and 10. Figure 9 displays the results on the energy spectra of neutrons produced in the ^{118}Sn + ^{28}Si fusion reaction at $E_{\rm lab}$=140 MeV. Solid dots with error bars in this figure represent experimental spectra of neutrons coincident with evaporation residues of atomic numbers A = 139–143, detected in the RMS focal-plane detector. The solid line is the result of a fit using the theoretical equation [35]

$$\frac{d\bar{m}}{dE_{\rm c.m.}} = \frac{\bar{m}}{\Gamma(n+1)} T^{-(n+1)} E^{n}_{\rm c.m.} \exp(-E_{\rm c.m.}/T) \qquad (1)$$

describing the energy-differential average neutron multiplicity ($\bar{m}$) in the rest frame of the emitter. In Eq. (1), the logarithmic-slope parameter T reflects an effective temperature along the decay cascade, related to but not identical [35,36] with the actual nuclear temperature of the first emitter nucleus in the cascade. The shape parameter n in this equation reflects the average number of cascade neutrons, such that in the one-neutron case ($n = 1$), the shape of the spectrum is Maxwellian. For an evaporation cascade of many neutrons, it has been shown [35] that $n = 0.45$ and the slope parameter $T = (11/12)T_m$, where T_m is the nuclear temperature of the first daughter of the compound nucleus. As seen in Fig. 9, the theoretical sequential-evaporation spectrum, calculated assuming $T = 1.71$ MeV and $n = 0.45$, gives an excellent account of the data. It also agrees very well with the results (dashed curve) of the statistical-model calculations using the code PACE [29]. In these PACE calculations, the yrast line was calculated according to the rotating liquid drop model, and the level density formula of Gilbert and Cameron [33] was used with a level density parameter of $a = A/8$ MeV^{-1} consistently along the decay cascade. The code default values were used for diffuseness of the entrance-channel angular momentum cutoff ($\Delta l = 2$), electromagnetic transition probabilities, and particle transmission coefficients. In Fig. 9, there is no indication of the presence of any noticeable preequilibrium component in the high-energy portion of the experimental spectrum, in excess of the yields expected theoretically for equilibrium evaporation.

In Fig. 10, angle-integrated neutron energy spectra are shown for decay cascades leading to individual evaporation residues of the indicated mass numbers identified by the RMS. The spectra for the $A = 139$ and 140 cases were summed to improve counting statistics. In all four cases displayed in Fig. 10, a simple theoretical evaporation spectrum (solid curves) parametrized by Eq. (1) accounts well for all of the experimentally observed yield. Also, the "full" statistical-model predictions (dot-dashed curves) obtained with the code PACE [29] using a common level density parameter scaling of $a = A/8$ MeV^{-1} agree well with the measured spectra.

In summary of the present observations for the ^{118}Sn + ^{28}Si fusion-evaporation reaction, it is concluded that the data sets from both types of experiments including neutron multiplicity distributions and neutron energy spectra are consistent with an assumption of a statistical evaporation from an equilibrated ^{146}Gd compound nucleus. There is no indication of a sizable preequilibrium neutron component, nor is there any noticeable influence seen of particular nuclear structure effects. The ^{118}Sn + ^{28}Si reaction appears to be well represented by the standard notions of compound nucleus formation and decay, in agreement with previous observations [7]. Therefore, this reaction can be regarded as a "reference" standard for comparison.

B. The ^{124}Sn + ^{28}Si reaction

A set of experimental data similar to the one for the "reference" reaction ^{118}Sn + ^{28}Si has been gathered for the ^{124}Sn + ^{28}Si fusion reaction at bombarding energies of $E_{\rm lab}$=120, 130, 140, and 150 MeV. The composite system ^{152}Gd, formed in these reactions with excitation energies ranging from 57 to 87 MeV, was found in several earlier studies [6,7,11] to exhibit certain decay anomalies. Experimental results obtained for this system in the present work, as well as the results of theoretical model calculations, are displayed in Figs. 11–14.

In Fig. 11, which is analogous to Fig. 8 for the "reference" reaction, values of the experimental (solid dots with error bars) first two central moments of the neutron multiplicity distribution from the ^{124}Sn + ^{28}Si reaction at several bombarding energies are compared with theoretical predictions made under various assumptions. As seen from a comparison of Figs. 11 and 8, for the neutron-rich system ^{124}Sn + ^{28}Si, both average multiplicities and variances of the multiplicity distributions are consistently larger than in the case of the neutron-poorer reference reaction. Qualitatively, such effects are expected from phase-space considerations, due to differences in neutron binding energies in the composite systems formed in the two reactions, as well as from the different competition from charged-particle evaporation.

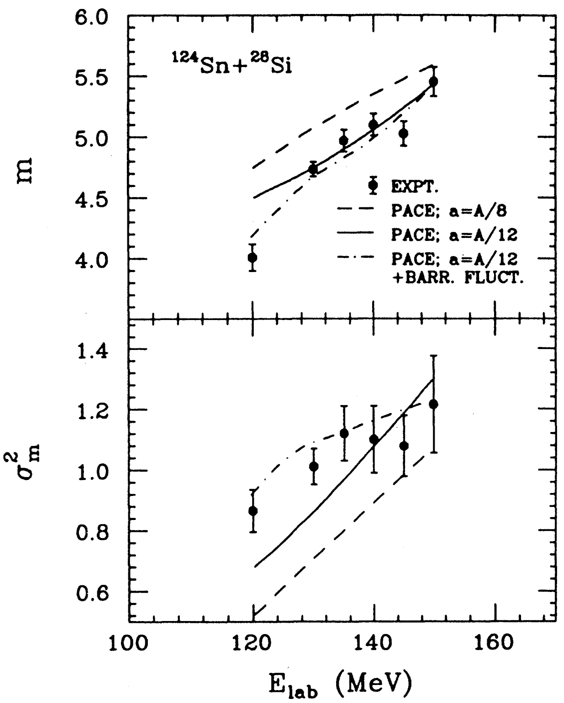

FIG. 11. Bombarding-energy dependence of the experimental first and second moments of the neutron multiplicity distribution for the ^{124}Sn + ^{28}Si reaction (solid symbols with error bars). The data are corrected for NMM efficiency and for background. The curves represent PACE calculations corrected for the finite acceptance of the ER detectors. See text for further explanation.

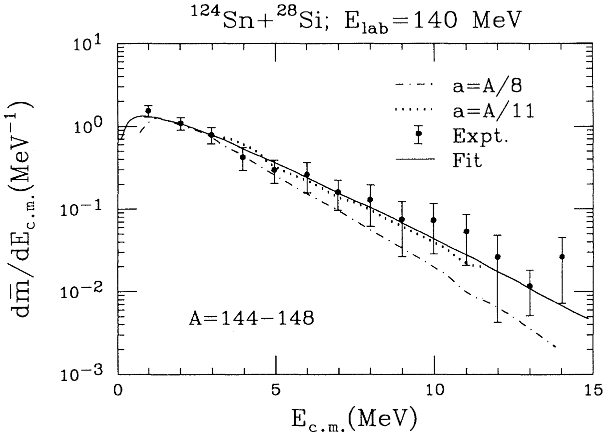

FIG. 12. Angle-integrated energy spectrum of neutrons from ER's with A = 144–148 from the reaction ^{124}Sn + ^{28}Si at $E_{\rm lab}$=140 MeV. The solid symbols are experimental data, while the solid curve represents a best fit obtained with Eq. (1). Dotted and dot-dashed curves are results of PACE calculations with level density parameters $a = A/11$ MeV^{-1} and $a = A/8$ MeV^{-1}, respectively.

Quantitatively, however, such an explanation is clearly insufficient, as demonstrated by the dashed curves in Fig. 11. The latter curves, significantly overpredicting the averages and underpredicting variances, represent results of statistical-model calculations using the code PACE [29] with the same systematic model parameters that were found satisfactory in the case of the ^{118}Sn + ^{28}Si reference reaction. In particular, the critical level density parameter in these calculations was assumed to be given by $a = A/8$ MeV^{-1}.

Given the success of theoretical model calculations in the cases of the ^{118}Sn + ^{28}Si, and several other reference reactions mentioned in Sec. II, the ^{124}Sn + ^{28}Si system can be considered to a certain extent as anomalous, in agreement with the conclusions of Stwertka *et al.* [7]. The present study, however, provides important clues as to the sources of the observed "anomaly," not available in the previous studies of similar systems. In particular, the observation of unexpectedly large variances of the neutron multiplicity distributions [Fig. 11(b)] points to unexpectedly high temperatures of the composite system along the decay cascade, a conclusion supported by relatively low average multiplicities. This observation, hence, invalidates the speculation put forward in the literature that the lower neutron multiplicities might be due to a diversion of the decay cascades into superdeformed bands, terminating prematurely neutron evaporation. If such bands of large collective energies (or any other collective modes) were to play any significant role in determining the particle evaporation patterns, their presence would effectively reduce the available thermal energy [37] and, hence, lower the emission temperatures, as well as the first two moments of the neutron multiplicity distribution. This was verified by PACE calculations employing an elevated yrast line. Such calculations proved unable to reproduce simultaneously both average and variance of the neutron multiplicity distribution for the system ^{28}Si+^{124}Sn. The observed anomaly cannot be explained by the enhanced γ transition strengths, either. As shown by Fornal *et al.* [34] for a slightly different reaction, the γ transitions have an effect mainly on the low-energy peak of the particle energy spectrum but change the spectral slope parameter only insignificantly. In contrast, both

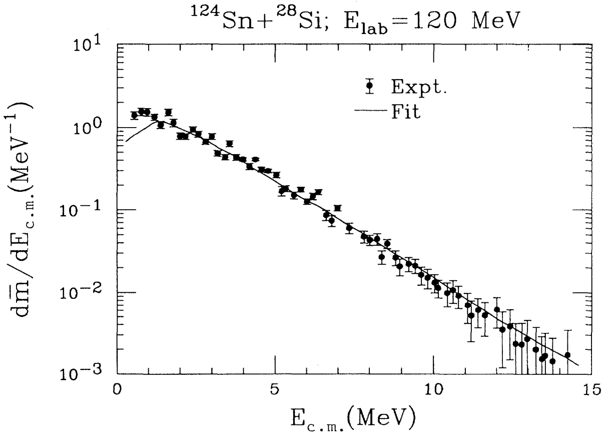

FIG. 13. Angle-integrated experimental spectrum (solid dots with error bars) of neutrons from ER's produced in the ^{124}Sn + ^{28}Si reaction at $E_{\rm lab}$=120 MeV. The solid curve represents the best fit obtained with Eq. (1), which also agrees with the prediction of a PACE calculation with level density parameters given by $a = A/12$ MeV^{-1}.

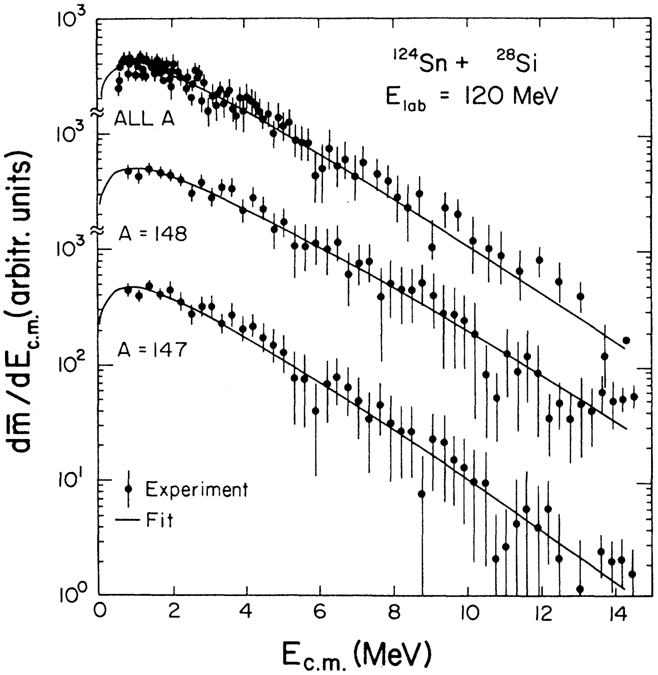

FIG. 14. Angle-integrated experimental (solid symbols) spectra of neutrons in coincidence with ER's produced in the ^{124}Sn + ^{28}Si reaction at $E_{\rm lab}$=120 MeV. The distributions are identified by the respective ER mass numbers. The solid curves represent best fits obtained with Eq. (1).

the observed neutron energy spectra and variances σ_m^2 require a significant increase in the effective temperature parameter.

In order to verify quantitatively that the experimental trends displayed in Fig. 11 are due to temperatures of the composite system that are higher than expected from systematics, model calculations were performed in which the level density parameters were decreased to $a = A/12$ MeV^{-1}, effectively raising the theoretical emission temperatures. Results of these calculations, shown in Fig. 11 by solid curves, are seen to provide a much better description of the data. A further improvement of the agreement between theoretical and experimental values of the first two moments of the neutron multiplicity distributions can be achieved by allowing for a diffuse cutoff of the compound nucleus spin distribution larger than the minimal value of Δl=0.5$\hbar$ assumed for the solid curves. Such rather large diffuseness is realistic at energies close to the fusion barrier of approximately 90 MeV [38–40]. The dot-dashed curves in Fig. 11 represent the results of the theoretical model calculations in which the diffuseness was increased to Δl=12$\hbar$. Such a value of the diffuseness parameter is compatible with the barrier-fluctuation systematics by Rossner *et al.* [39] predicting $\Delta l \sim 8\hbar$ at the present energies. At any rate, the much improved agreement of the dot-dashed curves with the experimental points in Fig. 11 indicates that, at least partially, the residual discrepancies between the theoretical solid curves and the experimental data could be due to effects of the spin distribution of the composite system, induced by fusion barrier fluctuations. Since such fluctuations are dependent on structure and neutron excess, it can be speculated that they are weaker in the case of low-energy fusion of the relatively neutron-poor system ^{118}Sn + ^{28}Si, where they lead to negligible effects in neutron multiplicity distributions. However, at present no quantitative support for this speculation can be offered. Although a more thorough discussion of the effects of barrier fluctuations on particle emission patterns is beyond the scope of this paper, the above sensitivity of the neutron (particle) multiplicity distribution suggests an independent and widely applicable method of studying such effects experimentally.

The important conclusion that the effective temperature of the composite system formed in the ^{124}Sn + ^{28}Si fusion reaction is higher than expected from the nuclear level density systematics, is unaffected by the above complication of the data points at the lowest bombarding energies. The value of the effective level density parameter a deduced from the NMM experiment is confirmed by the analysis of the data obtained in the TOF-RMS experiments on this system, as shown in Figs. 12–14.

In Fig. 12, the measured center-of-mass cumulative energy spectrum (solid dots with error bars) of neutrons from the fusion reaction ^{124}Sn + ^{28}Si at $E_{\rm lab}$=140 MeV, summed over the evaporation residue mass numbers A = 144–148, is compared with the results of various theoretical calculations. As in the case of the reference reaction ^{118}Sn + ^{28}Si of Figs. 9 and 10, the presence of any significant preequilibrium emission component can be excluded also for the ^{124}Sn + ^{28}Si reaction, and the spectrum of Fig. 12 can, therefore, be analyzed in terms of equilibrium evaporation from an excited composite system. The solid curve in this figure represents the best fit obtained using Eq. (1). It is seen to almost coincide with the results of the "full" statistical-model calculations (dotted curve) performed using the computer code PACE with a level density parameter scaling of $a = A/11$ MeV^{-1}, a value consistent with $a = A/12$ MeV^{-1} earlier found necessary to explain the neutron multiplicity distributions for this reaction. The dash-dotted curve in Fig. 12 represents the results of the statistical-model calculations with the level density parameter scaling of $a = A/8$ MeV^{-1} and a standard diffuseness of the angular momentum cutoff of Δl=2, consistent with the data from the reference reaction ^{118}Sn + ^{28}Si. The latter curve demonstrates the sensitivity of the neutron energy spectra to the level density parameter a.

Figure 13 shows energy spectra of neutrons in coincidence with evaporation residues from the ^{124}Sn + ^{28}Si reaction at $E_{\rm lab}$=120 MeV, a bombarding energy close to the fusion barrier. Again, no contribution from a preequilibrium emission source is seen, and the solid curve represents the theoretical prediction for equilibrium evaporation, obtained using $a = A/12$ MeV^{-1}. In this case, the best-fit [Eq. (1)] and PACE-calculation curves coincide. It is interesting to note that the same scaling of the level density parameter is deduced by Kühn *et al.* [6] for the ^{92}Zr + ^{64}Ni reaction.

For the most intensely populated evaporation residues ^{147}Gd and ^{148}Gd, inclusive energy spectra of neutrons were obtained with sufficiently good statistics. These are displayed in Fig. 14, together with the spectrum summed over all A values measured with RMS. The solid curves in this figure represent best fits obtained using Eq. (1), which required a spectral slope parameter of T = (1.83 ± 0.16) MeV and T = (2.05 ± 0.23) MeV for the cases of ^{147}Gd and ^{148}Gd, respectively. These two slope parameters agree with each other within their statistical uncertainty. They agree also with the average slope parameter of T = 2.09 MeV required to fit Eq. (1) to the theoretical spectrum as calculated with the code PACE and $a = A/12$ MeV^{-1}.

IV. SUMMARY AND CONCLUSIONS

The present work represents an attempt to explain aspects of neutron emission from the composite system ^{152}Gd formed in the heavy-ion fusion reaction ^{124}Sn + ^{28}Si that were previously found at variance with the established systematics of statistical decay of similar systems. A rich set of experimental data was collected by measuring, in two series of experiments and at several bombarding energies, both the exclusive energy spectra and the multiplicity distributions of neutrons coincident with massive evaporation residues. For comparison, similar data were collected for the "well-behaved" composite system of ^{146}Gd formed in the ^{118}Sn + ^{28}Si.

Energy spectra of neutrons emitted from both systems are well described by Maxwellian-like distributions over the whole range of bombarding energies $E_{\rm lab}$=120–140

MeV explored, with no indication on any significant role of preequilibrium emission mechanism. Average neutron energies are, however, systematically higher for ^{152}Gd than for the ^{146}Gd reference system, at a similar excitation energy per nucleon, and point to different scalings of the level density parameter a or a different specific heat along the decay paths of the two systems. While the decay of ^{146}Gd can be well understood assuming a parameter value of $a = A/8$ MeV^{-1}, a scaling according to $a = A/12$ MeV^{-1} is required, in order to explain the spectra of neutrons emitted from the ^{152}Gd system. This conclusion regarding different thermal characteristics is further confirmed by the systematic quantitative differences between the measured multiplicity distributions of neutrons emitted from the two systems. According to microscopic models, this difference in nuclear level densities can be traced back to a smaller effective density g of single-particle states at the Fermi surface for the nuclei in the evaporation chain originating in the ^{152}Gd composite than that for the daughters of ^{146}Gd.

While providing no microscopic explanation for the deduced difference in thermal properties of the two composite systems studied, the present results speak clearly against hypothesis attributing differences in the neutron emission patterns of ^{146}Gd and ^{152}Gd to the influence of superdeformed bands, which would be difficult to reconcile with Bohr's notion of a statistically equilibrated compound nucleus.

ACKNOWLEDGMENTS

The authors would like to thank Dr. R. W. Peelle and the Oak Ridge National Laboratory for making the NMM available to us. The kind hospitality and help received from Dr. R. Gwin, Dr. R. W. Ingle, and Dr. R. R. Spencer is deeply appreciated. Thanks are due also to M. Satteson who provided valuable help during the experimental runs involving the RMS. This work was sponsored by U.S. Department of Energy Grant No. DE-FG02-88ER40414. One of us (J.L.W.) acknowledges partial support by NSF Grant No. PHY-9109090.

[1] R. G. Stokstad, in *Treatise in Heavy-Ion Science*, edited by D. A. Bromley (Plenum, New York, 1984), Vol. 3, p. 81, and references therein.

[2] W. U. Schröder and J. R. Huizenga, in *Treatise in Heavy-Ion Science*, edited by D. A. Bromley (Plenum, New York, 1984), Vol. 2, p. 113, and references therein.

[3] *Nuclear Structure and Heavy-Ion Reaction Dynamics*, Proceedings of the Workshop on Interface Between Nuclear Structures and Heavy-Ion Reaction Dynamics, University of Notre Dame, 1990, edited by R. R. Betts and J. J. Kolata [Inst. Phys. Conf. Ser. **109**, (1991)].

[4] J. D. Garrett, G. B. Hagemann, and B. Herskind, Annu. Rev. Nucl. Part. Sci. **36**, 419 (1986), and references therein.

[5] D. Ward, H. R. Andrews, B. Haas, P. Taras, and N. Rud, Nucl. Phys. **A397**, 161 (1983).

[6] W. Kühn, P. Chowdhury, R. V. F. Janssens, T. L. Khoo, F. Haas, J. Kasagi, and R. M. Ronningen, Phys. Rev. Lett. **51**, 1858 (1983).

[7] P. M. Stwertka, T. M. Cormier, M. Herman, and N. G. Nicolis, Phys. Lett. **150B**, 91 (1985).

[8] P. M. Stwertka, T. M. Cormier, N. G. Nicolis, and M. G. Herman, Phys. Lett. **161B**, 70 (1985).

[9] C. Cabot, H. Gauvin, H. Sergolle, P. Aguer, G. Bastin, J. P. Thibaud, H. Delagrange, and Y. Patin, Z. Phys. A **322**, 393 (1985).

[10] A. Ruckelshausen, R. D. Fischer, W. Kühn, V. Metag, R. Mühlhans, R. Novotny, T. L. Khoo, R. V. F. Janssens, H. Gröger, D. Habs, H. W. Heyng, R. Repnow, D. Schwalm, D. Duchène, R. M. Freeman, B. Haas, F. Haas, S. Hlavac, and R. S. Simon, Phys. Rev. Lett. **56**, 2356 (1986).

[11] R. V. F. Janssens, R. Holtzmann, W. Henning, T. L. Khoo, K. T. Lesko, G. S. F. Stephans, P. C. Radford, A. M. van Denberg, W. Kühn, and R. M. Ronningen, Phys. Lett. B **181**, 16 (1986).

[12] D. J. Love, P. J. Bishop, A. Kirwan, P. J. Nolan, D. J. Thornley, A. H. Nelson, and P. J. Twin, Phys. Rev. Lett. **68**, 158 (1986).

[13] S. Henss, A. Ruckelshausen, R. D. Fischer, W. Kühn, V. Metag, R. Novotny, R. V. F. Janssens, T. L. Khoo, D. Habs, D. Schwalm, D. Freeman, G. Duchène, B. Haas, F. Haas, S. Hlavac, and R. S. Simon, Phys. Rev. Lett. **60**, 11 (1988).

[14] G. Smith, B. Haas, A. Alderson, I. Ali, C. W. Beausang, M. A. Bentley, P. Dagnall, P. Fallon, G. de France, P. D. Forsyth, U. Huttmeier, P. Romain, D. Santos, P. J. Twin, and J. P. Vivien, Phys. Rev. Lett. **68**, 158 (1992).

[15] P. J. Twin, B. M. Nyakó, A. H. Nelson, J. Simpson, M. A. Bentley, and H. W. Cranmer-Gordon, P. D. Forsyth, D. Howe, A. R. Mokhtar, J. D. Morrison, J. F. Sharpey-Schafer, and G. Sletten, Phys. Rev. Lett. **57**, 811 (1986).

[16] M. J. A. deVoigt, J. C. Bacelar, E. M. Beck, M. A. Deleplanque, R. M. Diamond, J. E. Draper, M. J. Riezebos, and F. S. Stephens, Phys. Rev. Lett. **59**, 270 (1987).

[17] F. S. Stephens, M. A. Deleplanque, J. E. Draper, R. M. Diamond, C. W. Beausang, W. Korten, W. H. Kelly, F. Azaiezm J. A. Becker, E. A. Henry, N. Roy, M. J. Brinkman, J. A. Cizewski, S. W. Yates, and A. Kuhnert, Phys. Rev. Lett. **64**, 2623 (1990).

[18] P. Taras, S. Flibotte, J. Gascon, B. Haas, S. Pilotte, D. C. Radford, D. Ward, H. R. Andrews, G. C. Ball, F. Banville, S. Cournoyer, D. Horn, J. K. Johansson, S. Monaro, N. Nadon, D. Prevost, C. Pruneau, D. Thibault, D. M. Tucker, and J. C. Waddington, Phys. Rev. Lett. **61**, 1348 (1988).

[19] S. Flibotte, H. R. Andrews, T. E. Drake, A. Galindo-Uribarri, B. Haas, V. P. Janzen, D. Prévost, D. C. Radford, J. Rodriguez, P. Romain, J. P. Vivien, J. C. Waddington, D. Ward, and G. Zwartz, Phys. Rev. C **45**, R889 (1992).

[20] D. G. Sarantites, C. Baktash, N. G. Nicolis, G. Garcia-Bermudez, V. Abenante, J. R. Beene, N. R. Johnson, M. L. Halbert, D. C. Hensley, F. K. McGowan, H. C. Griffin, I. Y. Lee, Z. Majka, M. A. Riley, T. M. Semkow, D. W. Stracener, and A. Virtanen, Phys. Rev. Lett. **64**, 2129 (1990).

[21] A. Galindo-Uribari, T. K. Alexander, H. R. Andrews, G. C. Ball, T. E. Drake, S. Flibotte, J. S. Forster, V.

P. Janzen, J. K. Johansson, N. Nadon, S. Pilotte, D. Prevost, D. C. Radford, P. Taras, J. C. Waddington, D. Ward, and G. Zwartz, Proceedings of the Workshop on Nuclear Structure and Heavy-Ion Reaction Dynamics [Inst. Phys. Conf. Ser. **109**, 179 (1990)].

[22] U. Jahnke, G. Ingold, D. Hilscher, H. Orf, E. A. Koop, G. Feige, and R. Brandt, *Detectors in Heavy-Ion Reaction*, Lecture Notes in Physics Vol. 179 (Springer, Berlin, 1983)

[23] S. S. Datta, Ph.D. thesis, Panjab University, 1989 (unpublished).

[24] J. Galin, X. M. Wang, E. Crema, D. Guerreau, D. X. Jiang, M. Morjean, J. Pouthas, F. Saint-Laurent, A. Sokolov, B. Gatty, D. Jacquet, B. Lott, U. Jahnke, E. Schwinn, E. Piasecki, and J. L. Charvet, in *Proceedings of the Symposium Heavy-Ion Collisions, Obernai, 1990*, edited by B. Heusch and H. Ishihara (World Scientific, Singapore, 1990).

[25] M. Morjean, H. Doubre, J. Galin, D. Guerreau, D. X. Jiang, J. Pouthas, J. L. Charvet, J. Frehaut, B. Lott, C. Magnago, Y. Patin, Y. Pranal, D. Jacquet, G. Ingold, and U. Jahnke, Nucl. Phys. **A524**, 179 (1991).

[26] D. Pade, W. U. Schröder, J. Tõke, J. L. Wile, and R. T. DeSouza, Phys. Rev. C **43**, 1288 (1991).

[27] J. Poitou and C. Signarbieux, Nucl. Instrum. Methods **114**, 113 (1974).

[28] J. Tõke and S. P. Baldwin, USDOE Progress Report No. ER40414-2, 1989, p. 218.

[29] M. Hillman and Y. Eyal (unpublished); A. Gavron, Phys. Rev. **21**, 230 (1980).

[30] R. A. Cecil, B. D. Anderson, and R. Madey, Nucl. Instrum. Methods **161**, 439 (1979).

[31] H. R. Bowman, S. G. Thompson, J. C. D. Milton, and W. J. Swiatecki, Phys. Rev. **126**, 2120 (1962).

[32] T. M. Cormier, Nucl. Instrum. Methods **1684**, 423 (1981).

[33] A. Gilbert and A. G. W. Cameron, Can. J. Phys. **43**, 1446 (1965).

[34] B. Fornal, F. Gramegna, G. Prete, G. D'Erasmo, E. M. Fiore, L. Fiore, A. Pantaleo, V. Paticchio, G. Viesti, P. Blasi, F. Lucarelli, M. Anghinolfi, P. Corvisiero, M. Taiuti, A. Zucchiatti, P. F. Bortignon, Ch. Ferrer, G. Nardelli, and G. Nebbia, Phys. Rev. C **42**, 1472 (1990).

[35] K. L. Lecouteur and D. W. Lang, Nucl. Phys. **13**, 32 (1959); **53**, 113 (1964).

[36] J. L. Wile, W. U. Schröder, J. R. Huizenga, and D. Hilscher, Phys. Rev. C **35**, 1608 (1987).

[37] T. R. Werner and J. Dudek, Phys. Rev. C **44**, R948 (1991).

[38] S. Gil, R. Vandenbosch, A. J. Lazzarini, D.-K. Lock, and A. Ray, Phys. Rev. C **31**, 1752 (1984).

[39] H. Rossner, J. R. Huizenga, and W. U. Schröder, Phys. Rev. C **33**, 560 (1986).

[40] R. Vandenbosch, Annu. Rev. Nucl. Part. Sci. **42**, 447 (1992).